Coordination chemistry of Ca sites at the surface of nanosized hydroxyapatite: interaction with H2O and CO

Bolis V.; Busco C.; Martra G.; Bertinetti L.; Sakhno Y.; Ugliengo P.; Chiatti F.; Corno M.; Roveri N.. Coordination chemistry of Ca sites at the surface of nanosized hydroxyapatite: interaction with H2O and CO. PHILOSOPHICAL TRANSACTIONS - ROYAL SOCIETY. MATHEMATICAL, PHYSICAL AND ENGINEERING SCIENCES. 370 (1963) pp: 1313-1336.
DOI: 10.1098/rsta.2011.0273

Coordination chemistry of Ca sites at the surface of nanosized hydroxyapatite: interaction with H_2O and CO

Vera Bolis,[a,*] Claudia Busco,[a] Gianmario Martra,[b] Luca Bertinetti,[b] Yuriy Sakhno,[b] Piero Ugliengo,[b] Fabio Chiatti,[b] Marta Corno,[b] Norberto Roveri.[c]

[a]*Dipartimento DiSCAFF, Università del Piemonte Orientale "A. Avogadro", Largo G. Donegani 2, I - 28100 Novara, Italy, INSTM (Italian National Consortium for Materials Science and Technology)-UdR Piemonte Orientale and NIS, Nanostructured Interfaces and Surfaces Centre of Excellence, Università degli Studi di Torino, Torino, Italy*

[b]*Dipartimento di Chimica IFM & NIS, Nanostructured Interfaces and Surfaces Centre of Excellence Università di Torino, Via P. Giuria 7, I - 10125 Torino, Italy, INSTM (Italian National Consortium for Materials Science and Technology)-UdR Università di Torino.*

[c]*Dipartimento di Chimica "G. Ciamician", Università di Bologna, Via Selmi 2, 40126 Bologna, Italy*

* to whom correspondence should be addressed:

Prof. Vera Bolis, E-mail address: vera.bolis@pharm.unipmn.it

Tel +39-0321-375-840; Fax +39-0321-375-621; Mobile +39-320-01-28-052

nanosized hydroxyapatite, H_2O adsorption, CO adsorption, microcalorimetry, IR spectroscopy, molecular modeling (*ab initio* calculations)

Submitted to Philosophical Transactions A for the themed issue "Structure and Activity of Bioceramics".

Abstract

The affinity towards water of a selection of well-defined, nanostructured hydroxyapatite samples (HA) was investigated by H_2O vapour adsorption microcalorimetry and IR spectroscopy. A large hydrophilicity of all investigated materials was confirmed. The surface features of hydrated HA were investigated on the as-synthesized samples pre-treated in mild conditions at T = 303K, whereas dehydrated HA features were characterized on samples activated at T = 573K. The relatively large hydrophilicity of the hydrated surface ($-\Delta_{ads}H$ ~100 – 50 kJ/mol) was due to the interaction of water with the highly polarized H_2O molecules strongly coordinated to the surface Ca^{2+} cations. At the dehydrated surface, exposing coordinatively unsaturated (*cus*) Ca^{2+} cations, H_2O was still molecularly adsorbed but more strongly ($-\Delta_{ads}H$ ~120-90 kJ/mol). The use of CO adsorption to quantify the Lewis acidic strength of HA surface sites revealed only a moderate strength of *cus* Ca^{2+} cations, as confirmed by both microcalorimetric and IR-spectroscopic measurements and *ab initio* calculations. This result implies that the large HA/H_2O interaction energy is due to the interplay between *cus* Ca^{2+} sites and nearby hydrophilic PO_4 groups, not revealed by CO probe. The lower density of *cus* Ca^{2+} cations at the 573K-activated HA surface with respect to the pristine one, did not affect the whole hydrophilicity of the surface, as the polarizing effect of Ca sites is so strong to extend up to the fourth hydrated layer, as confirmed by both high-coverage microcalorimetric and IR spectroscopic data. No specific effects due to the investigated specimens preparation method and/or different morphology were observed.

Introduction

Hydroxyapatite [HA, $Ca_{10}(PO_4)_6(OH)_2$] is the calcium phosphate phase thermodynamically stable in physiological environment, and is a key biomaterial in that both bioactive and bioresorbable. [1-3] Nanosized synthetic HA materials, which are largely employed for bones and teeth repair/replacement,[3] are generally accepted to be a good model system for biological hydroxyapatite, i.e., the mineral component of human bones and teeth enamel, as well as of several pathological calcifications.[4-6]

The ability of HA to favourably interact with living cells is also witnessed by the fact that HA grows at the bioactive glasses surface as a response of their interaction with (simulated) physiological body fluids, and allowing their integration within the living body.[2,7-9]

The unique features of HA as either natural or synthetic biomaterial have been extensively investigated during the years, see for instance refs.[1,2,10-16] and references therein. Only few papers, however, deal with the detailed structural features of HA surface, in spite of the key role played by the nature/structure of surface sites, involved in the molecular events occurring at the interface between biomaterials and physiological fluids.[3,17-19]

Much work has been devoted in recent years to optimize the preparation conditions of HA materials, by following a biomimetic approach in aqueous environment. [2,13,20-22] In particular, an innovative method to produce (at low temperature) nanometric, structurally well-defined and highly crystalline HA was recently set up and adopted.[10,23] The availability of well-defined nanostructured HA materials (synthesized in controlled and reproducible conditions) allowed to start investigating systematically the surface features of synthetic biomimetic apatite-like materials by means of the typical surface chemistry methods, which generally require (ultra) high vacuum techniques and well defined model systems.[3,17,18,24]

A multi-technique approach was previously employed by some of us to investigate the morphology (by UHR-TEM) and the surface features (by means of IR spectroscopy and thermogravimetry) of a variety of nanosized HA obtained by different biomimetic preparation methods.[25,26] UHR-TEM micrographs provided evidence that HA nanoparticles were made up by nano-crystals of either platelet-like or needle-like morphology (according to the temperature of the preparation procedure), in all cases elongated in the direction of the crystallographic *c*-axis. Still, according to the carefully controlled synthesis procedure, the nanoparticles crystalline core was either coated by an amorphous layer,[25] or was extended up to the surface.[26,27]

The interaction with H_2O and CO as probe molecules allowed to monitor the dehydration/rehydration features of thermally activated HA samples and the development of Lewis surface acidity at cationic surface sites. For the as-synthesized material, it was found that the first

hydration layer is essentially made up of H_2O molecules strongly bound to surface Ca^{2+} cations, in a 1:1 ratio. Conversely, hydroxyl groups accounted only for ~20% of surface hydration species. Outgassing at increasing temperatures up to T = 573K resulted in a complete, partially irreversible surface dehydration, accompanied by a decrease in the whole water adsorption capacity.

The surface structure of stoichiometric HA as such,[28] and in interaction with small molecules such as water [29,30] and glycine [30,31] was also studied by some of us by *ab initio* modeling, combined with experimental techniques (adsorption microcalorimetry and IR spectroscopy).

The present work is aimed at quantitatively describing the adsorption of H_2O_{vap} at the surface of the nanosized synthetic HA specimens already characterized by UHR-TEM and IR spectroscopy,[25,26] distinguished by the preparation conditions with consequent differences in morphological features.

The hydrophilicity of the surface was assessed by adsorption microcalorimetry on both pristine hydrated and thermally dehydrated HA samples. The Lewis acidic strength of the coordinatively unsaturated (*cus*) Ca^{2+} cations was quantified by means of the joint use of adsorption microcalorimetry and IR spectroscopy, and confirmed by *ab initio* modeling.

The investigation at molecular detail of the (quantitative) features of the adsorption of water at surface sites and within the multilayers approaching the liquid-like phase, is of greatest interest. In fact, water is ubiquitous in all body fluids and H_2O molecules are expected to play a major role in the complex interplay of water–biopolymer and surface–biopolymer interactions.[17,18] The more or less ordered arrangement of H_2O molecules at the solid biomaterial surface, which is a consequence of H-bonding, electrostatic and dipolar interactions induced by the specific distribution of surface sites, is also expected to play a role in the processes occurring at the biomaterials/body fluids interface.[32,33]

As for the role played by Lewis acidic surface cations in HA it is worth mentioning that the presence of Ca^{2+} cations in a regular geometric arrangement was proposed to be a key factor in HA surface-induced peptide folding.[34]

2. Experimental

2.1 Materials. A selection of nanosized hydroxyapatite samples of general formula $Ca_{10}(PO_4)_6(OH)_2$ were synthesized in aqueous environment (hydrothermal synthesis) according to the procedure described in ref.[26] consisting in dropping a solution of H_3PO_4 into a $Ca(OH)_2$ suspension to accomplish the following reaction:

$$5Ca(OH)_2 + 3H_3PO_4 \rightarrow Ca_5(PO_4)_3OH + 9H_2O$$

The individual reaction mixtures were stirred under N_2 in different conditions to obtain different kinds of materials; after stirring, slurries were left standing for ~2 h to ripen. The solid phase was

then separated by filtration from the mother liquor, repeatedly washed with distilled water and eventually dried in the chosen conditions (*vide infra*).

HA-am. One sample was prepared by mixing the reagents at T = 313K; the reaction mixture was stirred for 24 h and eventually freeze-dried. This material will be referred to as HA-am because made up the nanocrystals terminating in an amorphous 1-2 nm thick layer, as evidenced by UHR-TEM.[25]

HA-cry. Another set of samples was prepared, which comprises: (i) two samples (HA-cry-1 and HA-cry-2) produced in nominally identical preparation runs, implying stirring of the reaction mixture at T = 368K (24h) and subsequent freeze-drying; (ii) a third sample (HA-cry-3) obtained by stirring the reaction mixture at T = 298 K (24h). In this latter case, the material was dried at room temperature. HA samples from this second set of preparations will be referred to as HA-cry-X (X= 1,2,3) because possessing a crystalline structure extended up to the surface.[26,27]

A200/Ca8 and A200/Ca8P3. Two model systems were prepared by selectively introducing at the surface of an amorphous silica (Aerosil 200 from Degussa, A200) either Ca- or both Ca- and P-species, employing the incipient-wetness impregnation technique described in ref.[35]. The Ca-modified silica specimen (A200/Ca8; BET specific surface area SSA_{BET} = 130 ± 4 m^2/g) was prepared by gradually wetting the dry silica powder with a 0.31M $Ca(NO_3)_2 \cdot 4H_2O$ aqueous solution to achieve the following (nominal) surface composition: 92% SiO_2 and 8% CaO (by mol%). The Ca-P-modified silica specimen (A200/Ca8P3, SSA_{BET} = 170 ± 4 m^2/g) was obtained by impregnating a fraction of A200/Ca8 sample with a 0.15M H_3PO_4 aqueous solution, following the same procedure as described above. The (nominal) surface composition was: 89% SiO_2, 8% CaO and 3% P_2O_5 (by mol%). The wet powders were dried in air at T = 373K (24 h) and then calcined at T = 873K (2 h) to get rid of nitrates left from the preparation. The amounts of Ca species nominally present at the surface were ~6 and ~4 Ca^{2+}/nm^2 for A200/Ca8 and A200/Ca8P3, respectively. The amount of P species of A200/Ca8P3 specimen was ~3 P/nm^2.

All reagents, if not otherwise specified, were purchased by Sigma-Aldrich.

Thermal treatments. Prior to the adsorption experiments, the samples (as a loose powder for volumetric-calorimetric measurements, and pressed in self-supporting pellets for IR-spectroscopic experiments) were outgassed either overnight at T = 303K or 2h at T = 573K (residual pressure p $\leq 10^{-5}$ Torr; 1 Torr = 133.3 Pa). (i) Thermal pre-treatment at T = 303K ensured that only physisorbed species were eliminated by the surface, without affecting the nature/extent of surface hydrated layer (constituted by one coordinated H_2O molecule per Ca^{2+} cation).[25] (ii) Thermal pre-treatment at T = 573K, which ensured all Ca^{2+} cations exposed at the surface to be fully dehydrated and de-

carbonated, was found to induce major changes in the structure of the surface (*vide infra*) as described in details in refs.[25,26].

Nomenclature. In order to distinguish the investigated samples pre-treated at different temperatures, the short name of the individual samples will be followed by the activation temperature value. For instance HA-am/573 means HA-am sample outgassed at T = 573K.

Probe molecules. High purity N_2 (Specpure) and high purity CO (Praxair) were employed for adsorption measurements without any additional purification except liquid nitrogen trapping. Bidistilled water from ELGA Purelab ultra system was purified *in vacuo* and rendered gas-free by several "freeze-pump-thaw" cycles to be employed in both adsorption microcalorimetry and IR spectroscopic measurements.

2.2 Methods

2.2.1 Specific surface areas (SSA_{BET}) of the investigated samples were obtained by N_2 adsorption at T ~ 77K by employing an automatic apparatus (ASAP 2020, Micrometrics) following the well known BET model.[36] Before adsorption measurements, the samples were outgassed at T = 423K for ~3h (residual pressure p ~ 10^{-3} Torr), to get rid of all physisorbed species.

2.2.2 Adsorption microcalorimetry. The enthalpy change associated to the adsorption was measured at T = 303K by means of a heat-flow microcalorimeter (Calvet C80, Setaram, F) connected to a home-made high vacuum gas-volumetric glass apparatus (residual pressure p ≤ 10^{-5} Torr). A well-established stepwise procedure was followed,[37,38] that allowed to determine, during the same experiment and for subsequent small increments of the adsorptive, both adsorbed amounts and integral heats evolved, as a function of the increasing equilibrium pressure. This latter was monitored by a transducer gauge (Ceramicell 0-100 Torr, Varian). The volumetric-calorimetric set-up allowed all thermal treatments *in vacuo* as well as adsorption-desorption experiments to be carried out *in situ*.

(i) Adsorption of H_2O vapour. Adsorbed amounts will be plotted in the form of volumetric isotherms (n_{ads} vs. pH_2O). The calorimetric outputs (integral heats evolved during the adsorption, Q^{int}) were routinely processed to obtain the differential heats of adsorption ($q^{diff} = -\Delta_{ads}H$, kJ/mol), which quantify with a reasonable accuracy the energy of interaction of the molecular probe with the individual sites. The shape of ($-\Delta_{ads}H$) vs. n_{ads} plots depends on, and actually describes, the surface sites heterogeneity, while the extrapolation of the plots to vanishing coverage [$q_0 = -(\Delta_{ads}H)_0$] yields the enthalpy changes associated with uptake on the most energetic sites, expected to be active in the earliest stages of the adsorption. The $-(\Delta_{ads}H)_0$ quantities, of experimental origin, are conveniently and fruitfully compared with the interaction energy (binding energy, BE) of one

adsorbed molecule with individual model sites, as obtained through *ab initio* calculations.[29,30,37,39]

(ii) Adsorption of CO. In this case the isotherms are not reported for the sake of brevity. As for the enthalpies of adsorption, owing to the poor activity towards the adopted molecular probe of both HA and model systems surfaces, it was more convenient to plot the integral evolved heats Q^{int} as a function of the adsorbed amounts n_{ads} (expressed as CO μmol/m^2) and to determine graphically the ($q^{diff} = -\Delta_{ads}H$, kJ/mol) quantity, according to the procedure previously described by Bolis *et al*.[40] In both H_2O_{vap} and CO cases, the reversibility/irreversibility features of the process were investigated through adsorption-desorption-adsorption measurements. After the first run of adsorption was completed (hereafter termed to as ads. I), each sample was outgassed overnight ($p \leq 10^{-5}$ Torr) at the adsorption temperature, and a subsequent second run was performed (hereafter termed to as ads. II). The presence of an irreversible component was inferred by the non-coincidence of ads. I and ads. II isotherms. By subtracting ads. II curve from ads. I, the adsorbed fraction not removed by simple evacuation was evaluated. Ads. II component will be hereafter referred to as the *reversible* adsorbed phase, whereas (ads. I – ads. II) component as the *irreversible* one (in the adopted conditions).

2.2.3 Infrared spectroscopy. Infrared spectra of the investigated HA samples were performed in transmission mode on powders pressed in self-supporting pellets and placed in a quartz IR cell equipped with CaF_2 windows, designed to carry out spectroscopic measurements both at beam temperature (BT ~313K, the estimated temperature of the sample under IR beam) or at low temperature (~100K, by cooling with liquid nitrogen). The IR cell was connected to a conventional *vacuum* line (residual pressure $p \leq 10^{-5}$ Torr), allowing all thermal pre-treatments and adsorption-desorption experiments to be carried out *in situ*. A Bruker Vector 22 spectrometer (resolution : 4 cm^{-1}; detector: DTGS) was employed for spectra collection. Details on the measurements protocol, extensively described in refs. [25,26], will be given along the text and in Supplementary Information-SI.

2.2.4 Molecular modelling*: *computational details. All calculations were run with the *ab initio* CRYSTAL09 code,[41] and the B3LYP functional. Full optimization was carried out for the free chosen HA surfaces, whereas only the internal coordinates were optimized for CO adsorption, keeping the cell parameters fixed to those of free HA surfaces. All-electrons double-zeta polarized Gaussian basis sets were adopted for atomic species belonging to HA surfaces, whereas a VTZP quality basis set was adopted for CO molecule. Harmonic frequencies were computed for CO molecules, considered as a fragment, using a standard algorithm. Strength of the CO molecules/HA surfaces interaction was evaluated by calculating the binding energy (BE), defined as:

$$BE = E(HA) + E(CO) – E(HA/CO)$$

where E(HA), E(CO) and E(HA/CO) are the energies for optimized bare slab, free CO molecule and CO interacting with HA-Ca sites, respectively. BE values were corrected for both basis set superposition error (BSSE) and dispersion contribution. This latter term was added by correcting the final BE value with a London type formula, as proposed by Grimme.[42] A more detailed description of the computational methods is reported in Supplementary Information-SI.

3. Results and Discussion.

3.1 Chemical, textural and morphological features of the investigated HA materials. Ca/P ratios, (bulk) carbonate content, SSA_{BET} values, morphology and (primary) particles size of the investigated HA materials are reported in **Table 1**. Density of *cus* Ca^{2+} cations exposed at the surface of either HA/303 or HA/573 is also reported.

Please insert Table 1

As indicated in the table, all prepared HA materials are made up of nanometre-sized particles, in all cases elongated along the c-axis, and exhibit a Ca/P ratio close to the stoichiometric one (1.67).[43,44] Beside a few habit morphological differences (in length, width and thickness) among the platelet-like and needle-like materials, in all cases (010) faces were found to prevail by far over the (001) ones.[26] In the last two columns of the table, the population of Ca^{2+} cations exposed per nm^2 at the investigated HA surfaces are indicated. These values were obtained by measuring adsorbed water amount resisting outgassing at BT ~313 K (in that strongly coordinated to *cus* Ca^{2+} cations), and assuming a 1:1 Ca^{2+}:H_2O stoichiometry, as extensively described in refs.[25,26]. The value obtained for HA samples outgassed at BT (see column 7) is ~4.5 Ca^{2+}/nm^2 for HA-am, and slightly lower for HA-cry.[26] Such a value is in fairly good agreement with data reported by Kukura *et al.*,[45] for HA materials. The lower value obtained for HA-cry materials was most likely due the presence at the surface of carbonates-like species.

As for the samples activated at T = 573K, the population of *cus* Ca^{2+} cations exposed at the surface (and available for H_2O coordination when re-exposed to water vapour) turned out to be roughly halved with respect to the pristine surface (see column 8). In fact, the thermal pre-treatment at T = 573K (i.e., at a temperature much larger than the highest temperature experienced by HA samples during their synthesis and post-synthesis treatments) was found to induce dramatic changes in both nature and structure of the surface, as it was demonstrated in refs.[25,26]. A possible surface reconstruction in the 573K-activated sample was also confirmed by volumetric-calorimetric data for both HA-am and HA-cry-1 (data not reported for the sake of brevity). It is out of the scope of this paper to investigate the structural aspects of HA materials treated at T > 373K, but work is in

progress in order to elucidate the mechanism of surface reconstruction induced by thermal treatments.[46] It is worth mentioning that previous molecular modelling studies of some of us suggested that all the considered surfaces are rather rigid and inward displacements of the most exposed Ca cations do not occur.[29] However, taking into account that stoichiometric HA does not generally occur in biological systems,[3] the presence of surface defects in real materials is expected to play a major role in inducing surface reconstruction in either Ca-rich or P-rich dehydrated (010) and (001) surfaces. The presence of both bulk and surface carbonate species in real materials (see Table 1), not accounted for by our previous simulations, is also expected to have an influence on the overall behaviour of the investigated HA materials. The effect of such substitutions (throughout the crystal or limited to the surface region) can be crucial in determining both bulk and surface biomaterial chemical properties.

3.2. Coordination of H_2O on surface Ca^{2+}cations. In **Figure 1** volumetric isotherms (**section A**) and enthalpy of adsorption vs. uptake plots (**section B**) of H_2O vapour adsorbed at T = 303K on HA pre-outgassed at either T = 303K or 573K, are illustrated. Data for silica-based model systems, A200/Ca8 and A200/Ca8-P3, pre-outgassed at T = 573K, are also reported for comparison purposes.

Please insert Figure 1

3.2.1 Volumetric data: water uptake. By inspection of **section A** diagram, it is observed that for hydrated HA/303 specimens: (i) adsorbed amounts (expressed as H_2O molecules adsorbed, in average, per *cus* Ca^{2+} cation) are virtually the same for all samples in that all volumetric isotherms are coincident; (ii) as expected, the adsorption is fully reversible, as witnessed by the first and second run of adsorption coincidence (ads. I and ads. II, respectively). Conversely, the scenario dramatically changes for HA samples fully dehydrated (and de-carbonated) by pre-outgassing at T = 573K. In particular: (i) ads. I and ads. II isotherms are not coincident, indicating that in such a case H_2O adsorption is partially irreversible (some 20-30% of the total uptake); (ii) even though normalized to the individual number of surface Ca^{2+} cations (reported in Table 1), water uptake measured for HA-am/573 is (slightly) larger than for HA-cry/573, suggesting that the amorphous layer somehow modifies the H_2O/HA interaction; (iii) the three HA-cry ads. I isotherms are virtually coincident, and the same occurs for the ads. II ones, suggesting that different preparations and/or morphological/textural features for these specimens do not influence the hydrophilicity of the surface.

The affinity towards water of the silica-based model systems outgassed at T = 573K is much lower than for both HA-am and HA-cry, outgassed at T = 303K and 573K. In fact, the correspondent isotherms lie in the very bottom of the diagram, even though normalized to the amount of *cus* Ca^{2+}

cations nominally present at the surface (~6 for A200/Ca8 and ~4 for A200/Ca8P3). In both A200/Ca8 and A200/Ca8P3 cases an irreversible component was detected (hardly visible in the adopted scale) which amounts to ~20-30% of the total uptake for the two samples, respectively.

As for water uptake on the investigated HA materials, adsorbed amounts (per Ca^{2+} cation) on dehydrated HA/573 are significantly larger than on hydrated HA/303, in agreement with the presence at the dehydrated surface of *cus* Ca^{2+} cations acting as Lewis acidic sites,[25,26,29] which are expected to be strong hydrophilic sites. The hydrated HA/303 surface is conversely made up of H_2O molecules coordinated to the surface, which act as hydrophilic sites of medium strength in that they are able to bind a second layer of H_2O molecules *via* H-bonding. In **Table 2,** the adsorbed amounts at pH_2O ~6 Torr for both ads. I and ads. II (expressed as either H_2O molecules/nm^2 or H_2O molecules/Ca^{2+} cation) are reported for HA-am and HA-cry-1, the latter being representative for the three fully crystalline HA materials. For the sake of clarity, the population of Ca^{2+}cations exposed per nm^2 either at the pristine HA/303 surface or at the thermally treated HA/573 surface, already listed in Table 1, was repeated in Table 2. Data for A200/Ca8/573 and A200/Ca8P3/573 model systems are reported for comparison purposes. It is worth noting that, if water uptake is expressed as H_2O molecules adsorbed per unit surface area (nm^2) instead of per Ca^{2+} cation, the HA/303 and HA/573 isotherms become surprisingly similar. Volumetric isotherms per unit surface area are not reported here for the sake of brevity, but can be seen in Supplementary Information-SI. Discrepancy between the two ways to express adsorbed amounts stems in the dramatic change on *cus* Ca^{2+} cations population available for coordinating water (see Tables 1 and 2). In the following, being interested to the detailed molecular interpretation of water-apatite interaction, H_2O adsorption data (including the energetic ones, *vide infra* section B of Figure 1) will be discussed in terms of H_2O molecules adsorbed per Ca^{2+} cation.

Please insert Table 2

By inspection of **Table 2**, it turns out that: (i) at the hydrated HA/303 surface ~2 H_2O molecules/Ca^{2+} are adsorbed, which are completely eliminated by pumping off at the adsorption temperature; (ii) at the dehydrated HA/573 surface ~4 H_2O molecules/Ca^{2+} are adsorbed (4.5 vs. 3.9 H_2O/Ca^{2+} for HA-am and HA-cry, respectively); (iii) in this latter case the process was not fully reversible in that ~1 of the four molecules adsorbed per cation was not desorbed by simple outgassing at the adsorption temperature. Note that this irreversible adsorption component was quantified by the (ads. I – ads. II) difference; (iv) the amount of water adsorbed on A200/Ca8 and A200/Ca8P3 model systems was very little with respect to both HA/303 and HA/573, in spite of their nominally larger density of *cus* Ca^{2+} cations. This datum indicates that HA surfaces exhibit a

unique large affinity towards water. Less than one molecule per *cus* Ca^{2+} cation was taken up by both A200/Ca8 and A200/Ca8P3, only ~ one tenth of which were irreversibly held at the surface.

In order to represent water uptake on the differently pre-treated HA surfaces, a schematic view of H_2O molecules adsorbed per square nanometre (at pH_2O ~6 Torr) on hydrated and dehydrated surfaces, is reported in **Figure 2**. The figure is a 2-dimensional sketch representing the density of Ca^{2+} centres on the x-axis, and the number of H_2O molecules per Ca^{2+} cation on the y-axis. Note that the drawing does not represent the molecular structure of the interface layer in that specific interactions between H_2O molecules and HA surface and among adsorbed H_2O molecules are not illustrated in details. Hypothesis on the molecular structure of the interface layer will be discussed when describing the energetic aspects of the H_2O/HA interaction (*vide infra*). In the figure, the HA/303 and HA/573 different surface density of *cus* Ca^{2+} cations available for coordinating H_2O is outlined.

Please insert Figure 2

Outgassing of the as-synthesized pristine HA surface **(scheme a)** results in either a hydrated HA/303 **(scheme b)** or a dehydrated HA/573 surface **(scheme c)**. In **scheme (b)** drawing, every one of the ~4 Ca^{2+} cations exposed per nm^2 of the HA/303 surface coordinatively binds one H_2O molecule.[25,47] This *first* hydrated layer represents the hydrophilic sites assembly encountered by H_2O molecules approaching from the vapour phase. In this respect, adsorption on hydrated HA/303 surface does simply re-build the *multi*-layers of water adsorbed. The two H_2O molecules per Ca^{2+} cation adsorbed on the top of the *first* hydrated layer, as represented in **scheme (d)**, correspond to the fully reversible adsorption of ~2 H_2O molecules/Ca^{2+} cation measured on both HA-am/303 and HA-cry/303 (see Table 2). In summary, as it is highlighted by the **scheme (d)** grey region, under a water vapour equilibrium pressure of ~6 Torr, every HA/303 surface Ca^{2+} cation retains (in average) ~3 molecules of H_2O.

In **scheme (e)** drawing, H_2O adsorption at the dehydrated HA/573 surface is schematically illustrated. In this case, the hydrophilic surface sites (~2 *cus* Ca^{2+} cations/nm^2) are depicted as free to interact with H_2O molecules approaching from the vapour phase: the early stage of H_2O adsorption restores the *first* hydrated layer. On the top of this layer, up to three H_2O molecules were adsorbed per Ca^{2+} cation (**scheme f**) according to what reported in Table 2. Three of the ~4 H_2O molecules adsorbed per Ca^{2+} cation are reversibly adsorbed whereas ~1 of them is not desorbed upon evacuation, and remains irreversibly bound to the surface. It is reasonable to infer that the ~3 H_2O molecules/Ca^{2+} cation not eliminated during the desorption step are weakly bound (*via* H-bonding interactions) and contribute to the edification of physisorbed *multi*-layers. Conversely, the

~1 H_2O molecule irreversibly adsorbed per *cus* Ca^{2+} cation is strongly bound to the surface (*via* Lewis acid-base coordination) and contributes to the edification of the *first* hydrated layer on HA/573 (**scheme e**). Note that the restored *first* hydrated layer is less dense than the pristine HA/303 *first* hydrated layer represented in **scheme (b**). Nonetheless, in spite of the lower density of hydrophilic sites on HA/573 with respect to HA/303, the whole adsorption capacity of the Ca^{2+} cations exposed at the former surface is larger than that of the latter one, as highlighted in the grey zone of **schemes (d)** and **(f)**: ~4 vs. ~3 H_2O molecules adsorbed per Ca^{2+} cation, for HA/573 and HA/303, respectively. As a consequence, from the present data it was not possible to infer whether the *multi*-layers arrangement of physisorbed water too is less dense at the HA/573 than at the HA/303 interface. As a matter of fact, in order to describe from a structural point of view the features of physisorbed water at the HA surface (both as-such and thermally treated at T = 573K) a molecular dynamic approach should be employed.[32,33]

3.2.2 Calorimetric data: energetic aspects of the water-apatite interaction. In **section B** of Figure 1, the enthalpy of H_2O adsorption ($q^{diff} = -\Delta_{ads}H$) is plotted as a function of adsorbed amounts (n_{ads}) expressed as H_2O molecules adsorbed per Ca^{2+} cation. The curves interpolating the experimental points are exponential functions obtained as described in ref.[37,48]. The shape of the curves, in all investigated samples, is typical of highly heterogeneous surfaces in that the adsorption enthalpy decreases from a quite high zero-coverage value [$q_0 = (-\Delta_{ads}H)_0 \geq 100$ kJ/mol] down to a value approaching the latent enthalpy of liquefaction of water [$(-\Delta_{LIQ}H) = 44$ kJ/mol] only at high coverage. The enthalpy value being larger than 44 kJ/mol in all cases (including the silica-based model systems) and in the whole range of H_2O pressure examined, it was confirmed that all investigated samples are typical hydrophilic surfaces.[37,38]

The enthalpy values reported in the diagram do confirm that HA surfaces (both the hydrated HA/303 and the dehydrated HA/573) exhibit a larger hydrophilicity than silica-based model systems, for which the zero-coverage enthalpy of adsorption $(-\Delta_{ads}H)_0$ amounts only to ~80 kJ/mol. In this latter case the adsorption enthalpy decreases quite steeply with coverage, approaching ~44 kJ/mol at a coverage lower than ~1 H_2O molecule/Ca^{2+} cation. Possible differences between ads. I and ads. II are hardly detected, owing to the scarce water uptake (see Table 2).

As for the investigated HA materials, it is observed that: (i) in spite of the slight difference in water adsorption capacity per Ca^{2+} cation (see Fig. 1A and Table 2), the sites energy distribution is virtually the same for all HA-am and HA-cry surfaces, as witnessed by very similar enthalpy vs. uptake plots; (ii) reversible adsorption (ads. II) curves for dehydrated HA/573 surface lie slightly above the intrinsically reversible adsorption at the hydrated HA/303 surface (ads. I = ads. II curves).

Note that in all reversible adsorption cases, the initial enthalpy of adsorption is surprisingly high: $(-\Delta_{ads}H)_0$ ~100 kJ/mol.

In details, for the hydrated HA/303 surface: (i) the first H_2O molecule reversibly adsorbed per Ca^{2+} cation (**scheme b** of Figure 2), develops a quite high energy: $-\Delta_{ads}H$ ~100 – 65 kJ/mol. These values are unexpectedly high (at least in the early stage of adsorption) if we consider that they correspond to H-bonding interactions between H_2O molecules belonging to the *first* hydrated layer and H_2O molecules approaching from the vapour phase; (ii) the second of the ~2 H_2O molecules adsorbed per Ca^{2+} cation (**scheme d**), also develops an energy which is still quite large ($-\Delta_{ads}H$ ~65-52 kJ/mol) with respect to ($-\Delta_{LIQ}H$) = 44 kJ/mol. This is an indication that H_2O molecules coordinated to Ca^{2+} cations in HA are strongly polarized by the interaction with the Lewis acidic sites, and in turn exhibit a strong affinity towards water. We will come back to this peculiar effect of water adsorbed on HA (*vide infra* section 3.3). As for the dehydrated HA/573 surface: (i) adsorption of H_2O_{vap} restoring the *first* hydrated layer (one Ca^{2+}/H_2O, **scheme e** in Figure 2), is characterized by a quite high adsorption enthalpy ($-\Delta_{ads}H$ ~120–90 kJ/mol), suggesting that the Lewis acidic strength of *cus* Ca^{2+} cations is quite high; (ii) adsorption of a second H_2O molecule per Ca^{2+} cation on the top of the restored *first* hydrated layer (this latter represented in **scheme e**) develops a still high energy ($-\Delta_{ads}H$ ~90–75 kJ/mol), close to that measured for the reversible adsorption on HA/303; (iii) further adsorption of a third and a fourth H_2O molecule per Ca^{2+} cation (as represented in **scheme f**) is characterized by an enthalpy of adsorption still significantly larger than 44 kJ/mol: $-\Delta_{ads}H$ ~75–60 and ~60–55 kJ/mol for the third and the fourth adsorbed molecule, respectively.

In summary, from the whole set of volumetric and calorimetric data reported, it turns out that the interaction between HA surface and H_2O molecules is definitely strong, at both low and high coverage. The low-coverage enthalpy values ($-\Delta_{ads}H$ > 100 kJ/mol) measured for HA/573 should be compatible with the dissociation of water at the dehydrated surface sites. However, IR spectroscopy data definitely discarded the occurrence of dissociative processes at the surface of 573K-activated HA, as demonstrated in refs.[25,26]. Molecular modeling too demonstrated that water is molecularly adsorbed at the individual Ca^{2+} surface sites and confirmed that the energy of H_2O-Ca species interaction is quite high, in fairly good agreement with experimental data obtained for nanosized HA partially dehydrated (i.e. activated at T = 403K).[30]

3.3. Multilayers of adsorbed water at HA surface. Complementary insight on the features of adsorbed water, either coordinated at the *cus* surface Ca^{2+} cations or making up the physisorbed *multi*-layers, were obtained by IR spectroscopy. The H_2O molecules stretching mode signal, which is expected to be highly sensitive to the presence/extent of H-bonding interactions, was carefully

analysed, taking into account that it is generally accepted that the stronger is the H-bonding interaction, the broader becomes the band shape and the lower the spectral position of the maximum.[49] The present work results are illustrated in **Figure 3**, where the bulk liquid water profile (dotted line) is also reported for comparison. By following the procedure described in SI, the contribution to the overall spectral profile of the first and of the following H_2O molecules adsorbed per Ca^{2+} cation was determined (trace a and traces b-d, respectively). Note that trace (d) is present only for HA/573 in that only in this latter case up to four H_2O molecules/Ca^{2+} cation were adsorbed at pH_2O ~6 Torr.

Please insert Figure 3

H_2O molecules belonging to the *first* HA hydration layer (one H_2O/Ca^{2+} either intrinsically present at the HA/303 surface: trace a in **panel A**; or re-adsorbed at HA/573 surface: trace a in **panel B**) exhibit a similar νOH profile, characterized by a large broadness (full width at half maximum, FWHM: ~750 cm^{-1}), with the maximum of the band downshifted of ~300 cm^{-1} with respect to that of bulk liquid water. The features of the bands account for the large perturbation suffered by H_2O molecules owing to the strong interaction with HA surface. As far as the number of adsorbed H_2O molecules per Ca^{2+} cation increases, a progressive decrease of FWHM and a parallel upshift towards liquid water maximum was observed for both HA/303 and HA/573 (see traces b and c in panels A and B, respectively, correspondent to the adsorption of the second and third H_2O molecules/Ca^{2+} cation). Still, in physisorbed water profile both spectral position and band shape testifies the presence of H-bonding interactions among H_2O molecules stronger than in bulk liquid water, in agreement with what suggested by the adsorption enthalpy vs. uptake plots (*vide supra*, Figure 1B). In fact, the second layer H_2O molecules on both HA/303 and HA/573 interact with underneath layers molecules *via* H-bonding with $-\Delta_{ads}H$ > 44 kJ/mol. Eventually, the third H_2O molecule per Ca^{2+} site taken up by HA/303 and the third-fourth taken up by HA/573 were characterized by a νOH band virtually coincident with the bulk water spectral position (curve c in **panel A** and curves c, d in **panel B**), in agreement with the calorimetric datum. Indeed, as illustrated by the Figure 1B plot, the adsorption enthalpy approaches the latent enthalpy of liquefaction of water only after either ~3 or ~4 H_2O molecules per Ca^{2+} cation are adsorbed (in average) on HA/303 and HA/573, respectively.

Preliminary conclusions. By summarizing the whole set of reported data on H_2O adsorption, the restored (HA/573) *first* hydrated layer is somehow different from that of the pristine (HA/303) surface (compare Fig. 2 schemes d and b, respectively), confirming that major changes occurred at the surface as a consequence of thermal treatment at T = 573K. Both H_2O uptake and physisorbed

molecules polarization is larger on rehydrated HA/573 than on the pristine hydrated HA/303 surface. In particular, the lower density of *cus* Ca^{2+} cations available for H_2O coordination on HA/573 most likely causes the hydrated layer too to be less densely packed in this latter case, and consequently the reciprocal interactions among physisorbed water molecules is expected to be different in the two HA/303 and HA/573 cases.

The high enthalpy of adsorption of water at the HA/573 surface, at both low and high coverage, seem to suggest that *cus* Ca^{2+} cations behave as strong Lewis acidic sites, coordinating water molecules which in turn become so highly polarized to be able to interact *via* strong H-bonding interactions with the next water molecules approaching from the vapour phase. It is however worth mentioning that the H_2O/HA interaction is certainly more complex than that envisaged until now, because of the interplay between the coordination of H_2O onto *cus* Ca^{2+} cations and a network of H-bonds of variable strength with the basic oxygen atoms of surface PO_4 groups, as it has been demonstrated by some of us by computer simulation.[29,30]

Thus, in order to single out the specific contribution of coordination from the complex water-apatite interaction, which involves also hydrophilic PO_4 species, the Lewis acidic strength of HA surface cations was quantified by means of CO adsorption.

3.4 Lewis acidic strength of HA surface Ca^{2+} cations: characterization by CO adsorption.

3.4.1 Adsorption microcalorimetry and IR-spectroscopy data. CO is a soft Lewis base widely used to reveal Lewis acidic sites, as for instance *cus* metal cations, either located in zeolite nanopores or exposed at the surface of metal oxides.[50] CO molecules are in fact sensitive to electric fields generated by *cus* metal cations and, when adsorbed, give rise to a clear IR spectroscopic response. The nature of the interaction, either a simple electrostatic polarization, a plain σ-coordination or a σ-coordination accompanied by a π-back donation (typical this latter of d-block metal cations), is revealed by the CO adsorbed spectral position with respect of the free molecule in the gas phase. In the case of both simple electrostatic polarization and plain σ-coordination, the stretching frequency of CO adsorbed is upward shifted with respect to νCO_{gas} (2143 cm^{-1}). It is generally accepted that $\Delta\nu_{CO} = (\nu CO_{ads} - \nu CO_{gas})$ blue-shift gives a semi-quantitative indication of the strength of CO/M^{n+} cations interaction and thus of the electric field of the surface.[50] It has also been demonstrated, on the basis of a large set of calorimetric and IR spectroscopic data on *non d/d^0*metal cations (for which π-back donation is prevented), that in case of σ-coordination and/or electrostatic polarization, $\Delta\nu_{CO}$ is correlated to the measured enthalpy of adsorption ($-\Delta_{ads}H$).[51,52]

In **section A** of **Figure 4**, the integral heats evolved during CO adsorption (at T = 303K) are reported as a function of the increasing uptake for both dehydrated HA-am/573 and HA-cry-1/573 samples. Data for CO adsorption on model systems A200/Ca8/573 and A200/Ca8P3/573 are also

reported for comparison purposes. Experimental points for HA/573 samples were fitted by common linear regressions in the low and high coverage regions of the $Q^{int} = f(n_{ads})$ plot, according to two different ranges which can be distinguished in the plot. The derivative of the Q^{int} vs. n_{ads} functions, in the present case the slope of the two straight lines, corresponds to the differential heats of adsorption ($q^{diff} = -\Delta_{ads}H$), expressed in kJ/mol. Ca-modified silica experimental points, too, were interpolated by a common straight line, the slope of which represents the enthalpy of adsorption.

The measured enthalpy of adsorption for HA/573 is $-\Delta_{ads}H$ ~40 kJ/mol, which corresponds to the adsorption of CO on a little fraction of *cus* Ca^{2+} sites exposed at the surface. In fact, only ~0.10 CO molecules/nm^2 are taken up by the HA/573 surface, which correspond (under the reasonable assumption of the one-to-one adsorption for CO at Ca^{2+} sites) to ~0.05 CO molecules/Ca^{2+} cation, i.e., to less than one CO molecule adsorbed every 20 *cus* Ca^{2+} cations. This result definitely indicates that, in average, HA *cus* Ca^{2+} cations cannot be considered as strong Lewis acidic sites. The second branch of the curve corresponds to a quite low enthalpy of adsorption, the value of which ($-\Delta_{ads}H < 10$ kJ/mol) is hardly assigned to a specific CO/surface sites interaction. The same was observed for Ca-modified silica model systems, for which an even lower enthalpy of adsorption was measured (approaching the enthalpy of liquefaction of CO, $-\Delta_{LIQ}H = 6$ kJ/mol). Most likely, the local enrichment of CO in the closeness of the surface allowed the weakly adsorbed CO molecules to reciprocally interact.[50]

In s**ection B** of **Figure 4,** IR spectra of CO adsorbed on HA-cry-1/573 at either BT (panel B1) or T~100K (panel B2) are reported. Let us first consider the IR spectrum obtained at BT (T ~313K), i.e., in conditions of temperature close to the adsorption microcalorimetry measurements. Only one CO band located at $\nu CO = 2181$ cm^{-1} ($\Delta\nu CO = 38$ cm^{-1}) was observed. The νCO frequency shift is in good agreement with the measured adsorption enthalpy in that $\Delta\nu CO = 38$ cm^{-1} and $-\Delta_{ads}H$ ~40 kJ/mol are well correlated with respect to the "universal" curve reported by Bolis *et al.*[51]. The maximum intensity of the band attained under progressively increasing CO pressure is extremely low (panel B1, curve e) witnessing, in agreement with volumetric-calorimetric data, for the overall weakness of HA surface cations as Lewis acidic sites. Another family of surface sites weaker than the few *cus* Ca^{2+} cations sufficiently strong to bind CO at BT, was revealed by decreasing the IR spectroscopic experiment temperature down to T ~100 K (panel B2). The first dose of CO admitted on the cooled sample produced a band similar in spectral position and intensity to the maximum signal obtained at BT (trace a). Note the different ordinate scale in B1 and B2 panels: the intensities of curve (e) in panel B1 and curve (a) in panel B2 are the same. Then, by increasing pCO, another component developed at lower frequency, which rapidly became the by far dominating component of the spectrum (traces b-i). As far as the intensity of the band increased, a progressive red-shift

down to 2168 cm^{-1} was observed, most likely because of the presence of adsorbate-adsorbate interactions.[50] Similar results (not reported for the sake of brevity) were obtained for the other investigated HA materials.[26] As for the Ca-modified silica specimens, no IR spectra of CO adsorbed were recorded owing to the extremely scarce and aspecific interaction between CO and surface sites, as evidenced by microcalorimetry at T = 303K, i.e. at a constant temperature slightly lower than BT (beam T ~313K).

Please insert Figure 4

Briefly, CO adsorption revealed that the Lewis acidic strength of *cus* Ca^{2+} cations exposed at the HA surface is moderate and close to the acidic strength exhibited by *cus* Ca^{2+} sites exposed at the surface of transition δ- or γ-Al_2O_3. The interaction in this latter case was characterized by νCO = 2185 cm^{-1} ($\Delta\nu CO$ = 42 cm^{-1}) and a correlated enthalpy of adsorption ($-\Delta_{ads}H$ ~45 kJ/mol).[52,53] It is worth noting that Ca^{2+} cations exposed at the surface of an ionic oxide such as alumina behave as Lewis acidic sites of medium strength, opposite to what observed for Ca^{2+} cations exposed at the surface of a covalent oxide like silica, for which only a scarce and aspecific interaction was observed (see Figure 4A). Conversely, in the case of highly coordinatively unsaturated Ca^{2+} cations located in Y-zeolite supercages, the Lewis acid-base interaction was much stronger, as witnessed by both νCO and adsorption enthalpy significantly larger than for both HA and Ca-modified alumina [$\Delta\nu CO$ = 51 cm^{-1} and $-\Delta_{ads}H$ ~ 51 kJ/mol].[54]

3.4.2. CO modelling data. *HA surfaces.* The interaction of CO with *cus* Ca^{2+} cations exposed at the HA surface was investigated also by *ab initio* simulation. The HA surfaces chosen for the modeling study were the (001) and the (010) ones, both present in the experimental HA nanocrystals (see Table 1), with the latter being the dominant one.[26] The non-stoichiometric (010) surface, characterized by either Ca-rich or P-rich terminations, were also considered. Both (001) and the (010) surfaces were previously investigated by some of us by DFT methods, either free or interacting with water and glycine (see ref.[30] and references therein). It is here recalled that the stoichiometric (010) surface (i.e., possessing in both bulk and surface the same Ca/P ratio) was found to dissociatively adsorb H_2O at the pristine surface sites giving rise to new surface terminations (Ca-OH and P-OH). For that reason, taking into account that experimental HA nanocrystals are grown in aqueous environment, it was reasonably assumed that the actual (010) morphology on real crystals is represented by the water-reconstructed (010) surface, hereafter referred to as (010)R. Conversely, both Ca-rich and P-rich (010) surfaces, similarly to what observed for the (001) surface, were found not to dissociate water upon adsorption,[30] in agreement with what demonstrated by IR spectroscopy in real nanosized HA specimens.[25]

Interaction with CO. The (001), (010)R and both Ca-rich and P-rich (010) surfaces were studied in interaction with CO molecules through their most exposed Ca cations. In **Figure 5**, best views of the HA/CO optimized structures are illustrated. Geometries of the complexes, binding energies (BE) and CO vibrational stretching shifts with respect to the free molecule ($\Delta\nu$(CO)) are reported. Binding energies (BE^{C}-D) in units of kJ/mol are reported as bare numbers, whereas $\Delta\nu(CO) = (\nu(CO_{complex}) - \nu(CO_{gas}))$ shifts, in units of cm^{-1} are indicated in parenthesis. By inspection of the figure, it turns out that binding energies are very similar for (010)R (BE 36.2 kJ mol^{-1}) and Ca-rich and P-rich (010) surfaces (BE = 38.0 and 40.2 kJ/mol, respectively). A lower value was calculated for the (001) surface (BE = 29.2 kJ/mol). Note that a delicate balance of electrostatic, charge transfer and exchange repulsion plus the contribution coming from dispersion energy is responsible for differences in BE final values. As for CO vibrational shifts illustrated in Figure 5, they are all very similar ($\Delta\nu$(CO) comprised in the 45-40 cm^{-1} range), irrespective of the considered HA surface. This datum indicates that the polarizing effect of the surface sites on CO depends most of all on the degree of exposure of Ca sites, rather than on the nature and/or structure of the crystallographic surface.

Please insert Figure 5

In summary, both experimental (microcalorimetric and IR-spectroscopic) and *ab initio* modeling indicated that the Lewis acidic strength of surface Ca^{2+} cations in HA is not sufficiently large to justify alone the high H_2O adsorption enthalpy, both calorimetrically measured and calculated by *ab initio* computations.[30] It was thus confirmed that H_2O molecules are so strongly adsorbed at the HA surface because their coordination at *cus* Ca^{2+} cations is reinforced by the presence of a network of H-bonds with the basic oxygen atoms of PO_4 groups.[29] Note that in the case of Ca-modified silica, scarcely active towards water coordination, the presence of P species at the surface did not enhance the extent of the interaction (neither in terms of adsorbed amounts nor in terms of energy of interaction, *vide supra*)

4. Conclusions

The near room temperature adsorption of H_2O vapour at the surface of a variety of nanosized HA materials was investigated by adsorption microcalorimetry and IR spectroscopy. All the obtained results confirmed the large affinity towards water of HA surface, both as synthesized and thermally treated at T = 573K. The large hydrophilicity of HA materials is due either to the presence of a highly polarized hydrated layer (in the pristine HA/303 material) or to the presence of an assembly of Lewis acidic sites (*cus* Ca^{2+} cations) in HA/573. These latter species, which strongly bind H_2O molecules ($-\Delta_{ads}H$ ~120-90 kJ/mol) through the oxygen end without dissociating them, were found

to exhibit only a medium strength Lewis acidity, as witnessed by CO adsorption measurements and *ab initio* calculations. This result confirmed the "composite" nature of HA hydrophilic sites, made up of *cus* Ca^{2+} cations acting in synergy with hydrophilic PO_4 species located in the close vicinity and arranged in a specific geometrical configuration. In such a way the H_2O/Ca sites complexes are stabilized by a structured H-bonding network. These features are expected to have an implication in the HA/biomolecules interaction and consequently in the biological behavior of apatite-like materials. The properties of the surface hydrated layer are in fact a key factor influencing the interaction with proteins and other molecules present in the (physiological) fluids.[55,56] Both the molecular nature of strongly adsorbed water and the moderate Lewis acidic strength of Ca sites most likely allow the interaction between HA surface sites and biomolecules not to be destructive of the structural features of these latter.[18,24]

The possible HA surface influence on the structure of the first shells of liquid water in physiological fluids,[32,55,56] was witnessed by the influence of HA surface electric field extended up to the *multi*-layers of physisorbed water. In fact, the presence at the HA/water interface of several strongly ordered hydration layers, originated by a network of strong electrostatic/hydrogen bonds, was revealed by means of molecular dynamics simulation.[33]

The low density of *cus* Ca^{2+} cations at the surface of thermally treated HA/573 was found not to depress the hydrophilicity of the surface, the polarizing effect of which is extended up to the fourth hydrated layer, as confirmed by both high-coverage calorimetric ($-\Delta_{ads}H > -\Delta_{LIQ}H$ of H_2O) and IR spectroscopic (νOH profile perturbed by H-bonding interaction) data.

No specific effects due to either the preparation method or the different morphology of the investigated specimens were observed on the adsorption neither in the case of H_2O adsorption nor in that of CO, as confirmed by both experimental (calorimetric/IR spectroscopic) and theoretical work (*ab initio* modelling).

The major structural changes occurring at the surface of HA materials thermally treated at T > 373K require further investigations, aimed at better understanding the mechanism of surface reconstruction and at monitoring the fate of *cus* Ca^{2+} cations becoming inactive toward water coordination on thermally treated HA/573.

Acknowledgements.

This work was financially supported by the Italian Ministry MUR (Project COFIN-2006, Prot. 2006032335_004: "Interface phenomena in silica-based nanostructured biocompatible materials contacted with biological systems") and by Regione Piemonte-Italy (Project CIPE-2004: "Nanotechnologies and Nanosciences. Nanostructured materials biocompatible for biomedical applications" and NANOMAT project, 2006), whose contribution is gratefully acknowledged.

CB and YS kindly acknowledge CRT Foundation - ISI Foundation scientific committee for Lagrange startup scholarship, and San Paolo Foundation for PhD scholarship, respectively.

Supporting Information. (i) Figure SI-1 Volumetric isotherms (section A) and enthalpy of adsorption vs. uptake plot (section B) of H_2O adsorbed at T = 303K on HA samples pre-outgassed at either T = 303K or 573K. Note that adsorbed amounts are expressed in H_2O molecules/nm^2. (ii) Figure SI-2. IR spectra of the $\nu(H_2O)$ region of HA-cry-1 outgassed at either T ~313K (section A) or T = 573K (section B), and subsequently contacted with increasing $H_2O_{vap.}$ pressure. (iii) CO adsorption integral heats: linear fit parameters. (iv) Computational details.

Table 1. Chemical, textural and morphological features of the investigated HA materials.

Sample	Ca/P (at)	Bulk carbonate content (wt%)	SSA_{BET} [a] ($m^2 \cdot g^{-1}$)	Morphology	Size [b] length (along c-axis) × width × thickness (nm)	Ca^{2+}/nm^2 [c]	
						303 K	573 K
HA-am	1.64	~2	78 ± 4	platelet-like	50-150 × 10-70 × 20-40	4.5±0.5	1.8±0.3
HA-cry-1	1.65	~1	70 ± 4	platelet-like	40-100 × 40-100 × 5-10	3.7±0.5	2.0±0.3
HA-cry-2	1.65	~1	75 ± 4	platelet-like	40-100 × 40-100 × 5-10	3.7±0.5	2.0±0.3
HA-cry-3	1.67	~4	130 ± 6 (120 ± 6)	needle-like	40-100 × 5-15 × 5-10	3.5±0.5	2.0±0.4

[a] SSA_{BET} was measured on both 303K- and 573K-activated materials; only in HA-cry-3 case a (slightly) lower value was obtained for the 573K-activated sample (reported in parenthesis) with respect to the 303K-activated one.

[b] Based on TEM data. For samples HA-am, HA-cry-1 and HA-cry-2 see ref.[26], for HA-cry-3 see ref.[27].

[c] Determined as described in details in refs. [25,26]. Figures reported in columns 7 and 8 refer to the samples outgassed at either T = 303K or T = 573K, respectively.

Table 2 H_2O adsorption quantitative features (at pH_2O ~6 Torr) for the investigated nanosized hydroxyapatite (HA-am and HA-cry-1) and for model systems (A200/Ca8 and A200/Ca8P3), expressed as both H_2O molecules/nm^2 and H_2O molecules/Ca^{2+} cation. The number of Ca^{2+} cations exposed per nm^2 at the individual surfaces are indicated.

		H_2O/nm^2			H_2O/Ca^{2+}cation		
	Ca^{2+}/nm^2	ads.I	ads.II	ads.I - ads.II	ads.I	$^{+}$ads.II	ads.I - ads.II
HA-am/303	4,5	9.2	9.2	-----	2.0	2.0	-----
HA-am/573	1.8	8.3	6.4	1.8	4.5	3.5	~1
HA-cry-1/303	3.7	7.2	7.2	-----	2.0	2.0	-----
HA-cry-1/573	2.0	7.9	5.4	2.5	3.9	2.8	~1
ACA8/573	~6	4.4	3.2	1.2	0.75	0.52	~0.2
ACA8P3/573	~4	3.2	2.7	0.5	0.75	0.63	~0.1

Figures Captions

Figure 1. Volumetric isotherms (**section A**) and enthalpy of adsorption vs. uptake plot (**section B**) of H_2O vapour adsorbed at T = 303K on HA samples pre-outgassed at either T = 303K or 573K. Legend: HA-cry-1/303 (3, 1), HA-cry-1/573 (,, –); HA-cry-2/303 ((, &), HA-cry-2/573 (!, ∀); HA-cry-3/303 (>, <), HA-cry-3/573 (7, 8); HA-am/303 (Σ, Θ), HA-am/573 (Λ, M). Data for silica-based model systems A200/Ca8 (Ω, Ξ) and A200/Ca8-P3 (β, χ) pre-outgassed at T = 573K are reported for comparison. In all cases open symbols refer to ads. II run. Latent enthalpy of liquefaction of water: $-\Delta_{LIQ}H(H_2O)$.

Figure 2. Scheme (a): pristine untreated HA surface; **scheme (b)**: *first* hydrated layer (one H_2O molecule per Ca^{2+} cation) present at the HA/303 surface (~4 *cus* Ca^{2+}/nm^2); **scheme (c)** *cus* Ca^{2+}/cations (~2/nm^2) exposed at the HA/573K surface; **scheme (d)** edification of water *multi*-layers on HA/303; **scheme (e):** edification of *first* hydrated layer (one H_2O molecule per *cus* Ca^{2+} cation) on HA/573K; **scheme** (**f)**: edification of water *multi*-layers on HA/573. In **scheme (d)** and **scheme (f),** the average uptake per Ca^{2+} cation is highlighted as a grey region. Solid circles: Ca^{2+} cations available for water interaction; open circles: inactive Ca^{2+} cations towards water adsorption.

Figure 3. IR spectra of HA cry-1: contribution to the ν-OH region of water molecules per *cus* Ca^{2+} cation present at the surface outgassed at BT ~ 313K (**panel A**) and at T = 573K (**panel B**) and then progressively rehydrated by contact with H_2O vapour (up to ~15 Torr). Full line traces refer to: (a) first H_2O molecule coordinated per *cus* Ca^{2+} cation (*first* hydrated layer); (b) second H_2O molecule adsorbed (in average) per Ca^{2+} cation; (c) third H_2O molecule adsorbed (in average) per Ca^{2+} cation; (d) fourth H_2O molecule adsorbed (in average) per Ca^{2+} cation (only at HA/573 surface). Dotted line: IR spectrum of liquid water. Details on the extraction of traces (a)-(d) from the original spectra are reported in SI.

Figure 4. Section (A) Integral heats of adsorption ($Q^{int,}$ J/m^2) vs. CO uptake (μmol/m^2) at T = 303K on fully dehydrated HA-am (Λ) and HA-cry-1 (,) samples in comparison with A200/Ca8 (Ω) and A200/Ca8P3 (β) model systems. Experimental points for HA-am and HA-cry-1 were fitted by common linear regressions in the low and high coverage regions; for A200/Ca8 and A200/Ca8P3 samples by a common straight line, the slope of which represents the enthalpy of adsorption. **Section (B)** IR spectra of CO adsorbed at BT (**panel B1**) and at T ~100K (**panel B2**) on HA-cry-1. Lettering is in the sense of increasing CO pressure, from ~0.010 up to ~20 Torr. Spectra are reported after subtraction of the background (i.e., the spectrum of the sample before CO adsorption). Note the different scale on the Y axis of the two panels: trace (e) in panel B1 has the

same intensity as trace (a) in panel B2. All samples reported in both **sections A** and **B** were pre-outgassed at T = 573K.

Figure 5. Best views of the optimized structures between CO and the most exposed Ca site at the considered HA surface, both stoichiometric and defective. Binding energies (BE^{C}-D) in units of kJ/mol are reported as bare numbers; $\Delta\nu CO = (\nu CO_{complex} - \nu CO_{gas})$ shifts in unit of cm^{-1} are indicated in parenthesis.

References

(1) Dorozhkin, S. V. 2009 Calcium Orthophosphates in Nature, Biology and Medicine. *Materials* **2** 399-498.

(2) Roveri, N. & Palazzo, B. In *Nanotechnologies for the life Science. Tissue, Cell and Organ Engineering*; Kumar, C. S. S. R., Ed.; Wiley-VCH Verlag GmbH & Co. KGaA: Weinheim, 2006; Vol. 9, p 283-307.

(3) Jones, F. H. 2001 Teeth and bones: applications of surface science to dental materials and related biomaterials. *Surf. Sci. Rep.* **42**, 75-205.

(4) Lowenstam, H. A. & Weiner, S. 1989 *On biomineralization*, New York: Oxford University Press.

(5) Glimcher, M. J., Bonar, L. C., Grynpas, M. D., Landis, W. J. & Roufosse, A. H. 1981 Recent studies of bone mineral: is the amorphous calcium phosphate theory valid? *J. Cryst. Growth.* **53**, 100-19.

(6) Mann, S. 2001 *Biomineralization: principles and concepts in bioinorganic materials chemistry*, New York: Oxford University Press.

(7) Hench, L. L. 2006 The story of Bioglass. *J. Mater. Sci. Mater. Med.* **17**, 967-978.

(8) Kokubo, T. 1996 Formation of biologically active bone-like apatite on metals and polymers by a biomimetic process. *Thermochim. Acta* **280/281**, 479.

(9) Hench, L. L. & Wilson, J. 1993 *Introduction to Bioceramics*, Singapore: World Scientific.

(10) Iafisco, M., Palazzo, B., Marchetti, M., Margiotta, N., Ostuni, R., Natile, G., Morpurgo, M., Gandin, V., Marzano, C. & Roveri, N. 2009 Smart delivery of antitumoral platinum complexes from biomimetic hydroxyapatite nanocrystals. *J. Mater. Chem.* **19**, 8385-8392.

(11) Iafisco, M., Palazzo, B., Falini, G., Di Foggia, M., Bonora, S., Nicolis, S., Casella, L. & Roveri, N. 2008 Adsorption and Conformational Change of Myoglobin on Biomimetic Hydroxyapatite Nanocrystals Functionalized with Alendronate. *Langmuir* **24**, 4924-4930.

(12) Kandori, K., Miyagawa, K. & Ishikawa, T. 2004 Adsorption of immunogamma globulin onto various synthetic calcium hydroxyapatite particles. *J. Colloid and Interface Sci.* **273**, 406-413.

(13) Kandori, K., Fudo, A. & Ishikawa, T. 2000 Adsorption of myoglobin onto various synthetic hydroxyapatite particles. *Phys. Chem. Chem. Phys.* **2**, 2015-2020.

(14) Peroos, S., Du, Z. & de Leeuw, N. H. 2006 A computer modelling study of the uptake, structure and distribution of carbonate defects in hydroxy-apatite. *Biomaterials* **27**, 2150-2161.

(15) Almora-Barrios, N., Austen, K. F. & de Leeuw, N. H. 2009 Density Functional Theory Study of the Binding of Glycine, Proline, and Hydroxyproline to the Hydroxyapatite (0001) and (011#0) Surfaces. *Langmuir* **25**, 5018–5025.

(16) de Leeuw, N. H. 2010 Computer simulations of structures and properties of the biomaterial hydroxyapatite. *J. Mater. Chem.* **20**, 5376-5389.

(17) Castner, D. G. & Ratner, B. D. 2002 Biomedical surface science: Foundations to frontiers. *Surf. Sci.* **500**, 28-60.

(18) Kasemo, B. 2002 Biological surface science. *Surf. Sci.* **500**, 656–677.

(19) Tirrell, M., Kokkoli, E. & Biesalski, M. 2002 The role of surface science in bioengineered materials. *Surf. Sci.* **500**, 61-83.

(20) Tampieri, A., Sandri, M., Landi, E., Celotti, G., N., R., Mattioli-Belmonte, M., Virgili, L., Gabbanelli, F. & Biagini, G. 2005 HA/arginate hybrid composites prepared trough bioinspired nucleation. *Acta Biomaterialia* **1**, 343-351.

(21) Tampieri, A., Celotti, G. & Landi, E. 2005 From biomimetic apatites to biologically inspired composites. *Anal. Bioanal. Chem.* **381**, 568-76.

(22) Landi, E., Tampieri, A., Celotti, G., Langenati, R., Sandri, M. & Sprio, S. 2005 Nucleation of biomimetic apatite in synthetic body fluids: dense and porous scaffold development. *Biomaterials* **26**, 2835-2845.

(23) Palazzo, B., Walsh, D., Iafisco, M., Foresti, E., Bertinetti, L., Martra, G., Bianchi, C. L., Cappelletti, G. & Roveri, N. 2009 Amino acid synergetic effect on structure, morphology and surface properties of biomimetic apatite nanocrystals. *Acta Biomaterialia* **5**, 1241-1252.

(24) Kasemo, B. 1998 Biological surface science. *Curr. Opin. Solid State Mater. Sci.* **3**, 451-459.

(25) Bertinetti, L., Tampieri, A., Landi, E., Ducati, C., Midgley, P. A., Coluccia, S. & Martra, G. 2007 Surface Structure, Hydration, and Cationic Sites of Nanohydroxyapatite: UHR-TEM, IR, and Microgravimetric Studies. *J. Phys. Chem. C* **111**, 4027-4035.

(26) Sakhno, Y., Bertinetti, L., Iafisco, M., Tampieri, A., Roveri, N. & Martra, G. 2010 Surface Hydration and Cationic Sites of Nanohydroxyapatites with Amorphous or Crystalline Surfaces: A Comparative Study. *J. Phys. Chem. C* **114**, 16640-16648.

(27) Sakhno, Y., Iafisco, M., Roveri, N., Coluccia, S. & Martra, G. 2011 in preparation Effect of the preparation conditions on the surface and interface features of nanohydroxyapatites. *J. Mater. Chem.*

(28) Corno, M., Orlando, R., Civalleri, B. & Ugliengo, P. 2007 Periodic B3LYP study of hydroxyapatite (001) surface modelled by thin layer slab. *Eur. J. Mineral.* **19**, 757-767.

(29) Corno, M., Busco, C., Bolis, V., Tosoni, S. & Ugliengo, P. 2009 Water Adsorption on the Stoichiometric (001) and (010) Surfaces of Hydroxyapatite: A Periodic B3LYP Study. *Langmuir* **25**, 2188-2198.

(30) Corno, M., Rimola, A., Bolis, V. & Ugliengo, P. 2010 Hydroxyapatite as a key biomaterial: quantum-mechanical simulation of its surfaces in interaction with biomolecules. *Phys. Chem. Chem. Phys.* **12**, 6309-6329.

(31) Rimola, A., Corno, M., Zicovich-Wilson, C. M. & Ugliengo, P. 2008 Ab Initio Modeling of Protein/Biomaterial Interactions: Glycine Adsorption at Hydroxyapatite Surfaces. *J. Am. Chem. Soc.* **130**, 16181.

(32) Jena, K. C. & Hore, D. K. 2010 Water structure at solid surfaces and its implications for biomolecule adsorption. *Phys. Chem. Chem. Phys.* **12**, 14383-14404

(33) Zahn, D. & Hochrein, O. 2003 Computational study of interfaces between hydroxyapatite and water. *Phys. Chem. Chem. Phys.* **5**, 4004–4007.

(34) Capriotti, L. A., Beebe, T. P., Jr. & Schneider, J. P. 2007 Hydroxyapatite Surface-Induced Peptide Folding. *J. Am. Chem. Soc.* **129**, 5281-5287.

(35) Cerruti, M., Magnacca, G., Bolis, V. & Morterra, C. 2003 Characterization of sol-gel bioglasses with the use of simple model systems: a surface-chemistry approach. *J. Mater. Chem.* **13**, 1279-1286.

(36) Brunauer, S., Emmett, P. H. & Teller, E. J. 1938 Adsorption of Gases in Multimolecular Layers. *J. Am. Chem. Soc.* **60**, 309-319.

(37) Bolis, V., Busco, C. & Ugliengo, P. 2006 Thermodynamic Study of Water Adsorption in High-Silica Zeolites. *J. Phys. Chem. B* **110**, 14849-14859.

(38) Fubini, B., Bolis, V., Bailes, M. & Stone, F. S. 1989 The reactivity of oxides with water vapor. *Solid State Ionics* **32-33**, 258-272.

(39) Bolis, V., Busco, C., Aina, V., Morterra, C. & Ugliengo, P. 2008 Surface Properties of Silica-Based Biomaterials: Ca Species at the Surface of Amorphous Silica As Model Sites. *J. Phys. Chem. C* **112**, 16879-16892.

(40) Bolis, V., Maggiorini, S., Meda, L., D'Acapito, F., Turnes Palomino, G., Bordiga, S. & Lamberti, C. 2000 X-ray photoelectron spectroscopy and X-ray absorption near edge structure study of copper sites hosted at the internal surface of ZSM-5 zeolite. A comparison with quantitative and energetic data on the CO and NH3 adsorption. *J. Chem. Phys.* **113**, 9248-9261.

(41) Dovesi, R., Saunders, V. R., Roetti, C., Orlando, R., Zicovich-Wilson, C. M., Pascale, F., Civalleri, B., Doll, K., Harrison, N. M., Bush, I. J.*et al.* In *CRYSTAL09 (CRYSTAL09 User's Manual)*; University of Torino: Torino, 2009.

(42) Grimme, S. 2006 Semiempirical GGA-Type Density Functional Constructed with a Long-Range Dispersion Correction. *J. Comput. Chem.* **27**, 1787-1799.

(43) Nancollas, G. H. 1982 *Biological Mineralization and demineralization*, Berlin: Springer.

(44) Le Geros, R. Z. & Le Geros, J. P. 1984 *Phosphate Minerals*, New York: Springer.

(45) Kukura, M., Bell, L. C., Posner, A. M. & Quirk, J. P. 1972 Radioisotope determination of the surface concentrations of calcium and phosphorus on hydroxyapatite in aqueous solution. *J. Phys. Chem. B* **76**, 900-904.

(46) Bolis, V., Busco, C., Martra, G., Bertinetti, L., Ugliengo, P., Chiatti, F., Corno, M. & Roveri, N. in preparation

(47) Bertinetti, L., Tampieri, A., Landi, E., Bolis, V., Busco, C. & Martra, G. 2008 Surface Structure, Hydration and Cationic Sites of Nanohydroxyapatite. *Key Eng. Mater.* **361-363**, 87-90.

(48) Aina, V., Bonino, F., Morterra, C., Miola, M., Bianchi, C. L., Malavasi, G., Marchetti, M. & Bolis, V. 2011 Influence of the Chemical Composition on Nature and Activity of the Surface Layer of Zn-Substituted Sol-Gel (Bioactive) Glasses. *J. Phys. Chem. C* **115**, 2196-2210.

(49) Eisenberg, D. & Kauzmann, W. 1969 *The structure and properties of water*, London, UK: Oxford University Press.

(50) Hadjiivanov, K. I. & Vayssilov, G. N. 2002 Characterization of oxide surfaces and zeolites by carbon monoxide as IR probe molecule. *Adv. Catal.* **47**, 307-511.

(51) Bolis, V., Barbaglia, A., Bordiga, S., Lamberti, C. & Zecchina, A. 2004 Heterogeneous Nonclassical Carbonyls Stabilized in Cu(I)- and Ag(I)-ZSM-5 Zeolites: Thermodynamic and Spectroscopic Features. *J. Phys. Chem. B* **108**, 9970-9983.

(52) Bolis, V., Magnacca, G. & Morterra, C. 1999 Surface properties of catalytic aluminas modified by alkaline-earth metal cations: a microcalorimetric and IR-spectroscopic study. *Res. Chem. Interm.* **25**, 25-56.

(53) Bolis, V., Cerrato, G., Magnacca, G. & C., M. 1998 Surface acidity of metal oxides. Combined microcalorimetric and IR-spectroscopic studies of variously dehydrated systems. *Thermochim. Acta* **312**, 63-77.

(54) Bolis, V., Fubini, B., Garrone, E., Giamello, E. & Morterra, C. In *Structure and Reactivity of Surfaces*; Morterra, C., Zecchina, A., Costa, G., Ed.; Elsevier: Amsterdam, 1989; Vol. 48, p 159-166

(55) Vogler, E. A. In *Water in Biomaterials Surface Science*; Morra, M., Ed.; John Wiley & Sons Ltd.: Chichester, 2001.

(56) Vogler, E. A. In *Biomaterial Science: An Introduction to Materials in Medicine*; Ratner, B. D., Schoen, F. J., Lemons, J. E., Eds.; Elsevier Inc.: San Diego, CA, 2004.

Figure 1

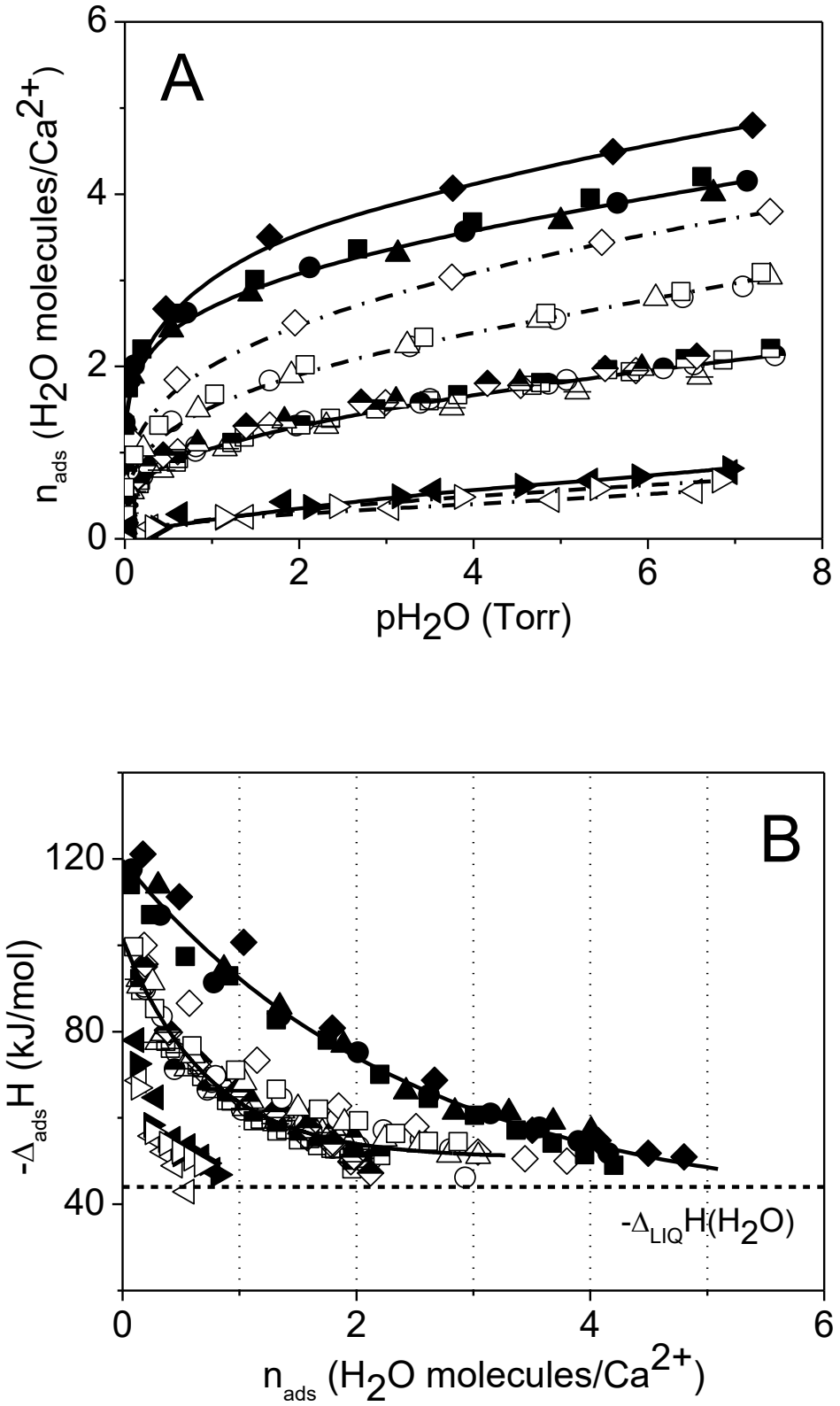
A
n_{ads} (H_2O molecules/Ca^{2+})
pH_2O (Torr)
B
$-\Delta_{ads}H$ (kJ/mol)
n_{ads} (H_2O molecules/Ca^{2+})
$-\Delta_{LIQ}H(H_2O)$

Figure 2

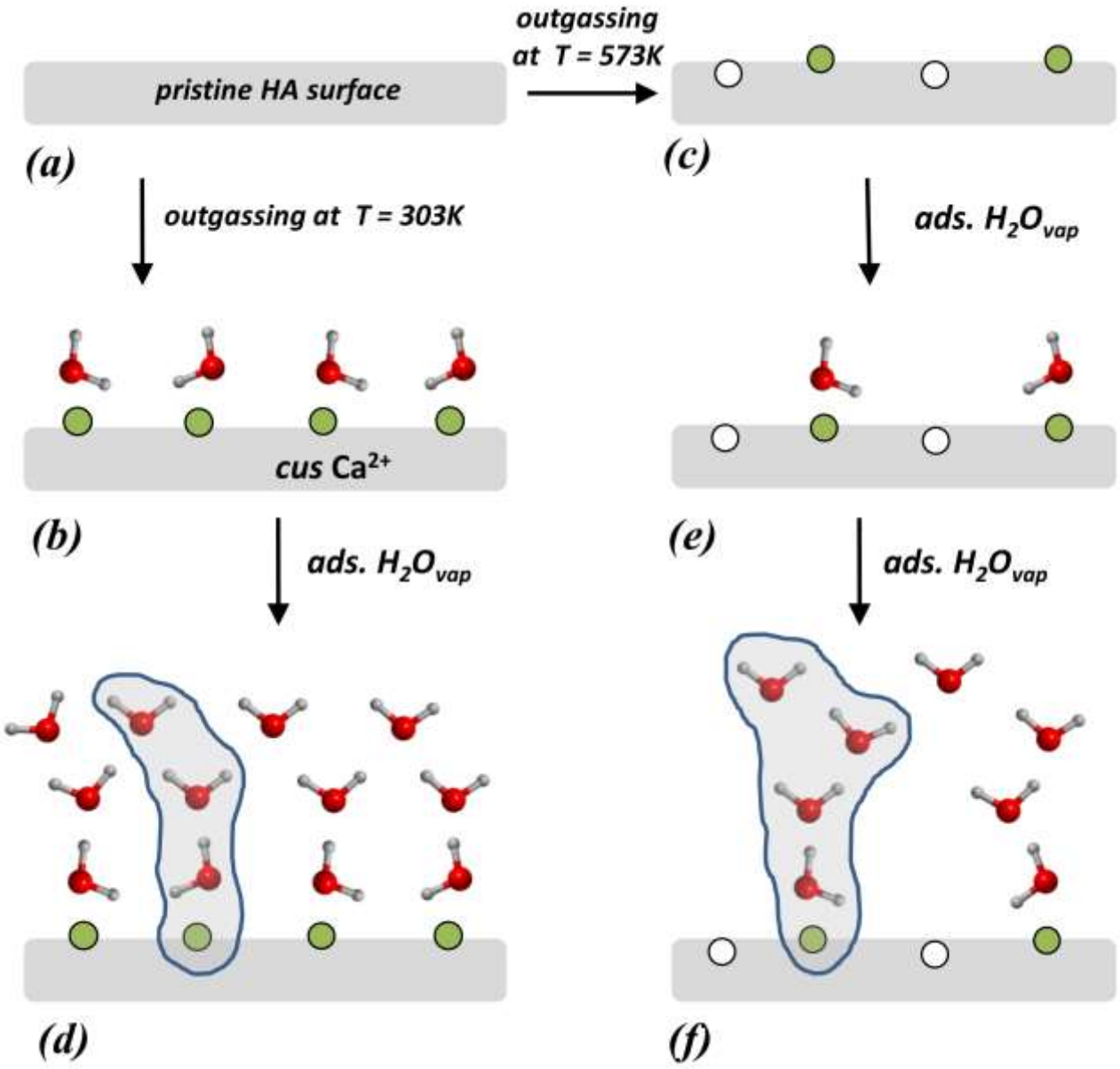
outgassing
at T = 573K
pristine HA surface
(a)
(c)
outgassing at T = 303K
ads. H_2O_{vap}
cus Ca^{2+}
(b)
(e)
ads. H_2O_{vap}
ads. H_2O_{vap}
(d)
(f)

Figure 3

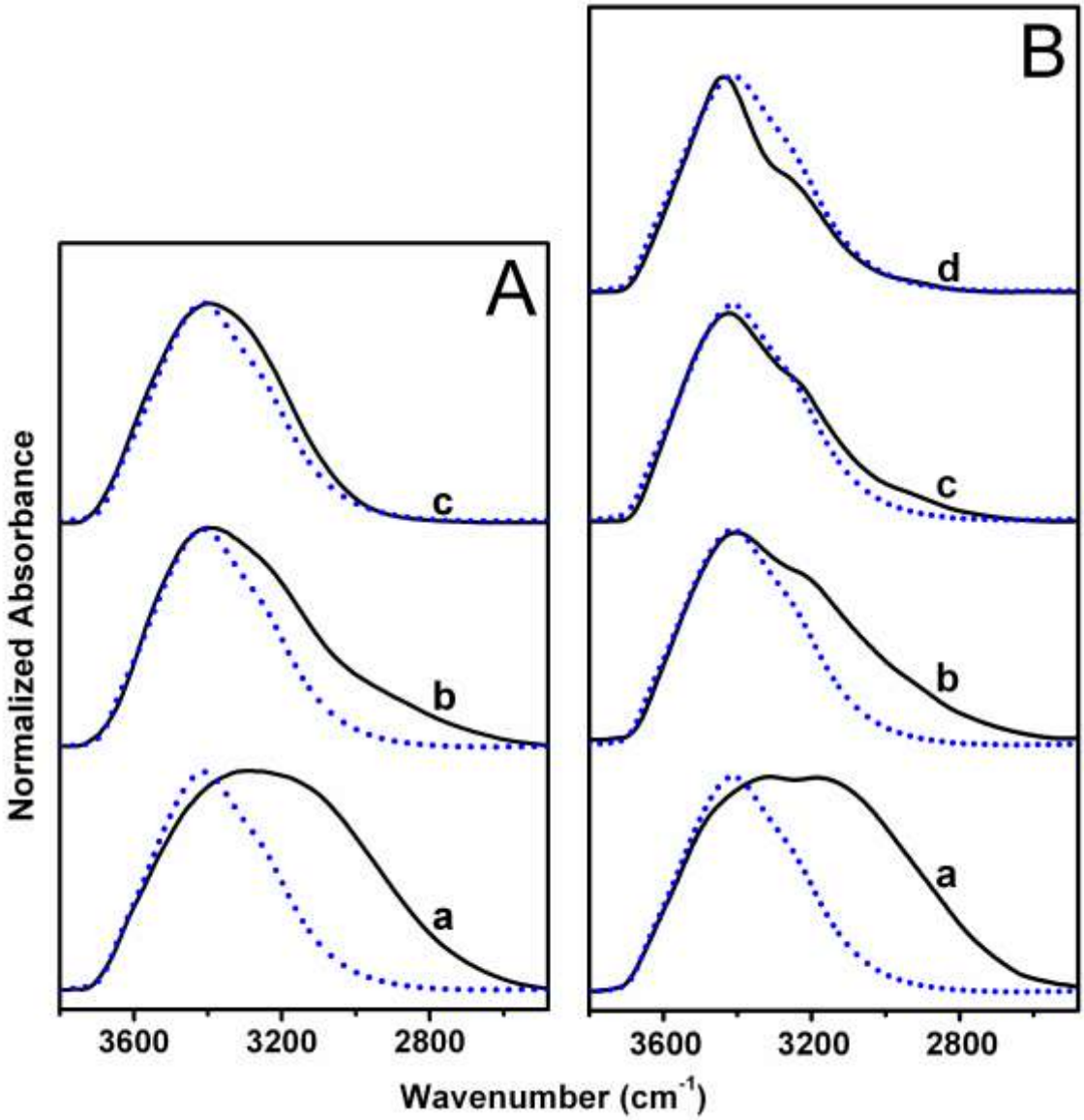
A
B
a
b
c
d
Normalized Absorbance
3600
3200
2800
Wavenumber (cm-1)

Figure 4

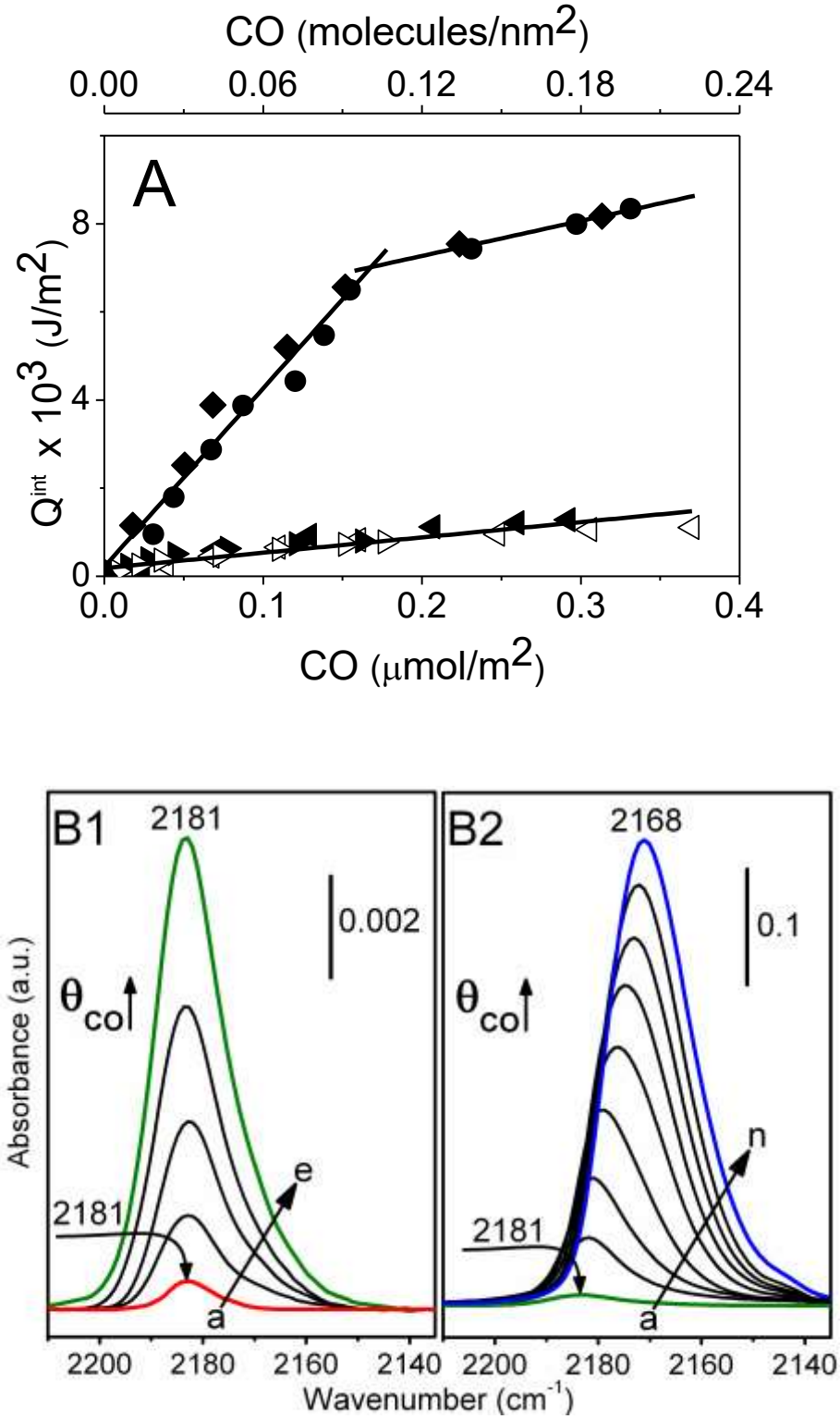
CO (molecules/nm2)
0.00
0.06
0.12
0.18
0.24
A
8
4
0
Qint x 10^3 (J/m2)
0.0
0.1
0.2
0.3
0.4
CO (μmol/m2)
B1
2181
0.002
θco
2181
e
a
B2
2168
0.1
θco
2181
n
a
Absorbance (a.u.)
2200
2180
2160
2140
Wavenumber (cm-1)

Figure 5

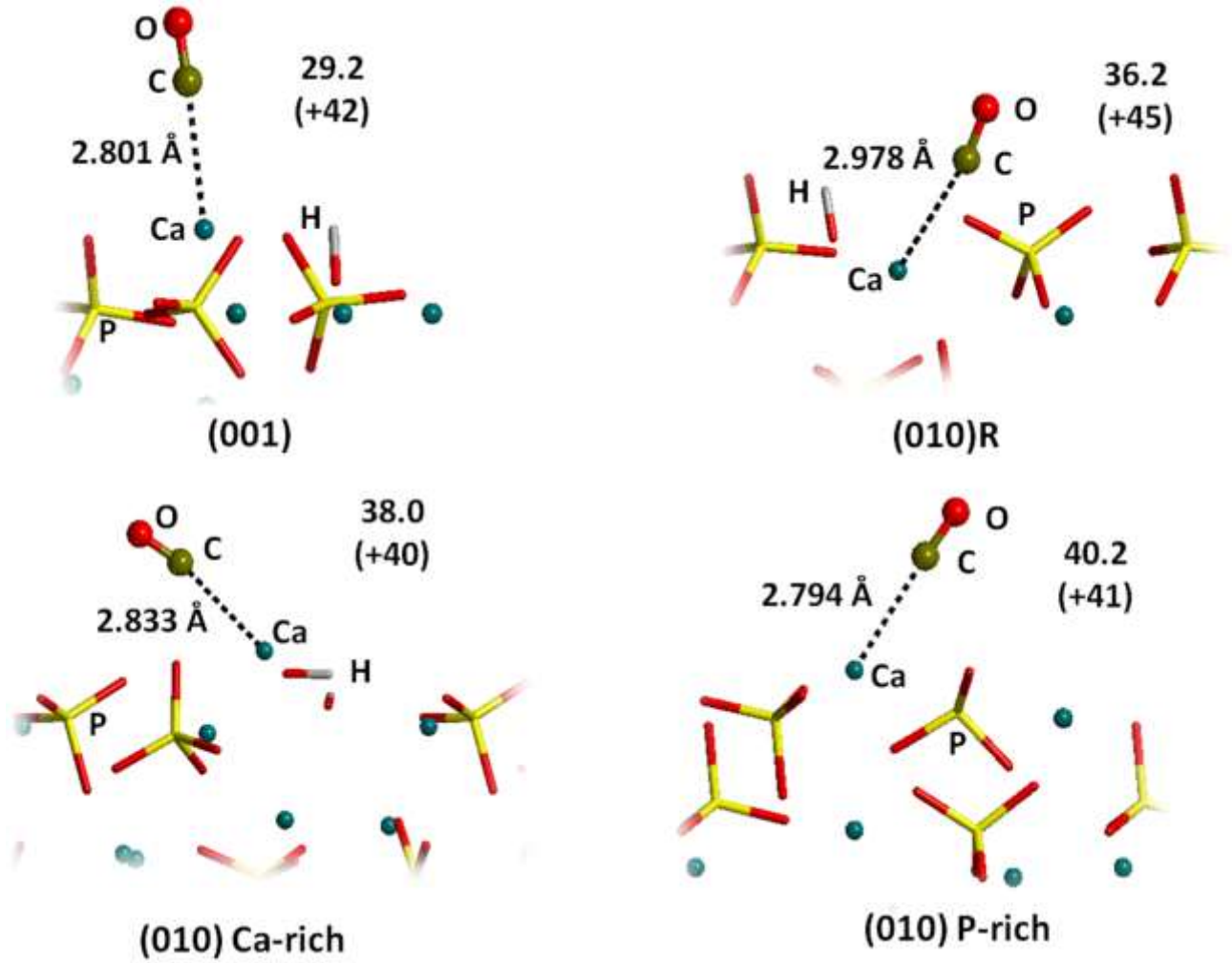
O
C
29.2
(+42)
2.801 Å
Ca
H
P
(001)
36.2
(+45)
O
2.978 Å
C
H
P
Ca
(010)R
O
C
38.0
(+40)
2.833 Å
Ca
H
P
(010) Ca-rich
O
C
40.2
(+41)
2.794 Å
Ca
P
(010) P-rich